Kresling origami actuator with embedded electromagnetic actuation

Kortman, V.G.; Hompes, J.T.; Sakes, A.; Jovanova, J.

DOI
10.1088/1361-665X/ade105

Publication date
2025

Document Version
Final published version

Published in
Smart Materials and Structures

Smart Materials and Structures

PURPOSE-LED PUBLISHING™

PAPER • **OPEN ACCESS**

Kresling origami actuator with embedded electromagnetic actuation

To cite this article: Vera Gesina Kortman *et al* 2025 *Smart Mater. Struct.* **34** 065018

OPEN ACCESS
IOP Publishing
Smart Materials and Structures
Smart Mater. Struct. **34** (2025) 065018 (9pp)
https://doi.org/10.1088/1361-665X/ade105

Kresling origami actuator with embedded electromagnetic actuation

Vera Gesina Kortman[1,2,*], Jouke Thomas Hompes[2], Aimée Sakes[1] and Jovana Jovanova[2]

[1] Department of BioMechanical Engineering, Delft University of Technology, 2628 CD Delft, The Netherlands
[2] Department of Maritime and Transport Technology, Delft University of Technology, 2628 CD Delft, The Netherlands

E-mail: v.g.kortman@tudelft.nl

Received 24 February 2025, revised 21 May 2025
Accepted for publication 4 June 2025
Published 17 June 2025

Abstract

In nature, organisms such as the octopus exhibit remarkable adaptability by reconfiguring their bodies into contracting and extending segments. Translating this modularity into robotics, origami-inspired designs have proven effective in creating adaptable building blocks for modular robotic arms. The Kresling cylinder, a bistable cylindrical origami structure, exemplifies this approach by functioning as both a contracting and extending actuator. However, current actuation strategies in origami-inspired structures—such as pneumatic, mechanical, or stimuli-responsive methods—suffer from bulky actuators, slow speed, or inability to provide local actuation. Magnetically-actuated Kresling cylinders offer promising solutions for rapid and localized actuation. However, they typically rely on large external coils, limiting their use in restricted environments. To overcome this limitation, we have embedded coils directly into a modular Kresling cylinder, creating a standalone electromagnetically-actuated system. The finite element analysis was employed to understand the effect of the electromagnets' dimensions on effective contraction and extension, resulting in a weight-efficient actuator. Trends were uncovered for the design of flat, effective electromagnets for embedded electromagnetic actuation. Following these design trends, a prototype was successfully manufactured, demonstrating rapid contraction and extension in both horizontal and vertical orientation. The standalone Kresling actuator is particularly well-suited for use in dynamic, remote or restricted environments. The simple design of the manufactured prototype illustrates the potential for incorporating embodied actuation into functional soft robotic designs.

Keywords: electromagnetism, Kresling origami, actuator, soft robot, embodied intelligence, bio-inspired design

* Author to whom any correspondence should be addressed.

1. Introduction

In nature, organisms with soft bodies, such as the octopus or the earthworm, exhibit remarkable adaptability in response to their environment. The octopus, for example, can change the shape of its arms by individually controlling different segments, creating local contracting, extending or bending segments. This ability allows the octopus to actively alter the shape of its arms to reach or fetch targets effectively.

This inherent flexibility and modularity contrasts with traditional robotic arms, which are typically constructed from rigid materials and have limited adaptability. This rigidity presents significant challenges when these robotic arms are employed in confined or narrow spaces. Applications such as logistical pick-and-place operations, vehicle manufacturing and inspection, or the cleaning and maintenance of restricted areas encounter difficulties due to the inflexibility of conventional robotic designs [1]. Consequently, dividing a robotic arm into flexible segments that can both extend or retract, depending on the environment, holds considerable potential for advancing robotic technology in these demanding environments.

Typical soft modular robotic arms integrate pneumatic linear actuators, such as bellows or McKibben muscles, to adapt their configuration in response to environmental demands [2–4]. However, the bulky nature of these pneumatic components, including the necessary pumps, limits the compactness of the arm, thereby affecting its manoeuvrability. Additionally, the need for an airtight system imposes constraints on the design freedom of the arm and increases its risk of operational vulnerabilities caused by leakages. Soft linear actuators that operate through alternative mechanisms, such as temperature-based actuation, encounter challenges related to lengthy cooling times, which can hinder their efficiency in dynamic applications. Furthermore, soft robotic arms often experience deflection due to loading, sometimes even from their own body weight, as they lack bearing capacity [5].

In the field of robotics, origami-inspired designs have demonstrated significant benefits in creating lightweight, deployable and tunable robots [6, 7]. Origami patterns that form thin-walled cylinders can fold into a compact shape while maintaining lateral stiffness during deployment. One notable example is the Kresling cylinder, a bistable and cylindrical-shaped origami structure. A Kresling cylinder can be described as a triangulated cylindrical origami composed of repeated triangular surfaces, with each unit cell consisting of one valley and one mountain crease line (figure 1) [8]. This configuration allows the cylinder to have two stable states: (1) a folded (contracted) disc-shaped state and (2) an unfolded (extended) cylindrical-shaped state [9]. The transformation between these states occurs through linear motion, showcasing the potential of the volume-efficient Kresling cylinder to act as a soft linear actuator. The Kresling cylinder is of particular interest because of its bending resistance when fully unfolded. In this state, the folding lines become tensioned, locking the structure into a more rigid form. This enhances its load-bearing capacity while still allowing smooth transitions between the folded and unfolded states.

Origami-inspired structures currently employ various actuation methods, including pneumatic, mechanical and stimuli-responsive actuation. These actuation strategies often result in bulky actuators, scaling issues, delicate components, slow speed, or inability to provide local actuation [6, 9–12]. The latter hinders the development of a modular robotic arm where, like an octopus arm, individual segments can effectively and independently contract or extend. Alternatively, Novelino *et al* [6] developed a magnetically-actuated Kresling system demonstrating precise and rapid elongation and contraction. Although this design negates many of the challenges currently faced with alternative actuation methods, these magnetically-actuated structures require generating a large magnetic field by surrounding coils. This requirement prevents the Kresling structure from acting as a standalone system, limiting its use in applications where external coils cannot be placed, such as in remote or restricted environments. It would be beneficial to embed the coils into the design of the Kresling actuator to initiate contraction or extension locally. The goal of this study is, therefore, to develop a standalone electromagnetically-actuated linear Kresling actuator, suitable for integration in a robotic arm.

2. Actuator design

2.1. Design direction

A schematic of the developed electromagnetic Kresling actuator is shown in figure 1. This actuator consists of a Kresling cylinder positioned between two electromagnets, each comprising a copper coil and a ferromagnetic core. The copper coils are connected to a power source with the electric current running in opposite directions, resulting in coils with opposite polarities. By alternating the electric current, the Kresling actuator can either contract or extend. The most challenging operational orientation of the Kresling actuator is vertical, as it must generate sufficient electromagnetic force to overcome its own weight during contraction. To ensure optimal performance, the produced electromagnetic force must exceed the combined weight of the actuator and the folding resistance of the Kresling cylinder. This underscores the importance of designing weight-efficient electromagnets to effectively actuate the Kresling cylinder. In the remainder of this study, the performance of the Kresling actuator is evaluated by its contraction efficiency (η). This efficiency is defined as the difference between the generated electromagnetic force (F_{m}) and the opposing forces, where the opposing forces are identified as the gravitational force of the actuator (F_{g}) and the folding resistance of the Kresling cylinder (F_{kresling}), as in (1). Here, the electromagnetic force is defined as the net magnetic interaction between the two electromagnets, arising from the force exerted on each magnet by the magnetic field of the other. In this study, the electromagnetic force is evaluated with the electromagnets positioned at their maximum separation, as this is the most critical case during the actuator's motion.

$$\eta = \frac{F_{\mathrm{m}} - F_{\mathrm{g}} - F_{\mathrm{kresling}}}{F_{\mathrm{g}} + F_{\mathrm{kresling}}}. \tag{1}$$

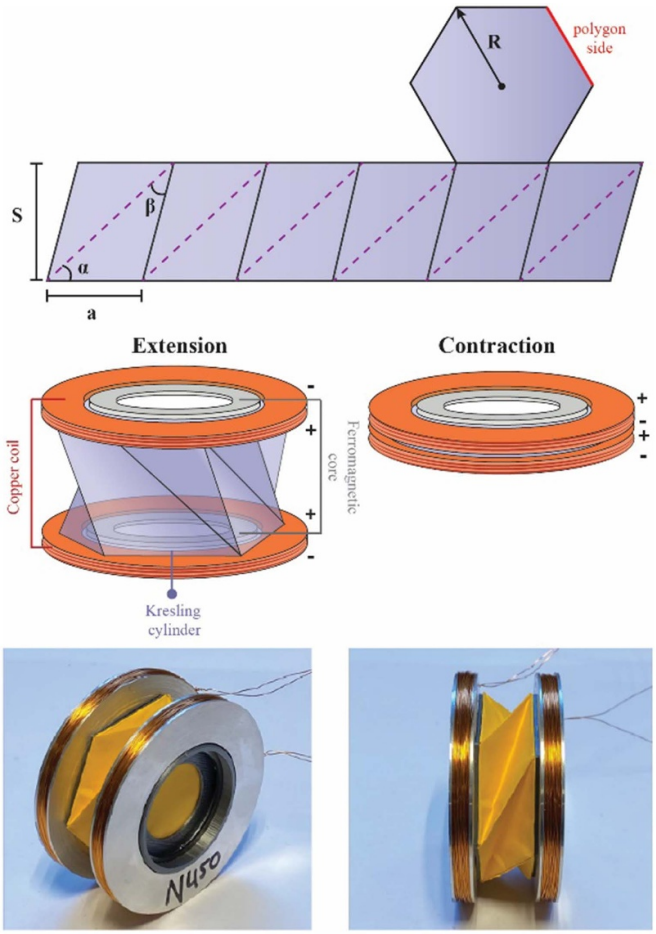

Figure 1. Overview of the electromagnetic Kresling actuator. Top: Folding pattern of the Kresling cylinder indicating the stroke length S, polygon side length a, triangle angles α and β and polygon radius R. The purple dotted lines resemble the valley crease lines, while the black solid lines resemble mountain lines. Middle: Schematic overview of the actuator in extension and contraction. Bottom: Prototyped actuator.

2.2. Kresling cylinder

The folding pattern of a Kresling cylinder is shown in figure 1. Two parameters can be used to characterize the Kresling cylinder, namely the polygon side length (a) and the stroke length (S). The polygon side length depends on the radius of the polygon (R) and the number of polygon sides (m), see (2). Consequently, the stroke length of the Kresling cylinder (S) can be determined by the polygon side length and angles α and β, as in (3).

$$a = 2\mathrm{R}\sin\left(\frac{\pi}{m}\right) \tag{2}$$

$$S = a\left(\sin(\alpha)\cos(\alpha) + \frac{\sin^2(\alpha)}{\tan(\beta)}\right). \tag{3}$$

For an optimized contraction efficiency (η), it is key to minimalize the folding resistance of the cylinder. To achieve this, the main dimensions of the Kresling cylinder are designed to minimize energy dissipation during folding. Wang *et al* [13] found that a Kresling configuration with angles $\alpha = 30°$ and $\beta = 30°$ exhibits minimal folding resistance. Additionally, Moshtaghzadeh *et al* [14] found that the stability of the Kresling cylinder increases with a higher number of polygon sides (m). However, an increased number of polygon sides also reduces the stroke length, as described by (2) and (3), resulting in a less efficient linear motion. Thus, a trade-off should be made between stroke length and stability of the Kresling cylinder. To act as proof-of-concept during this study, a Kresling cylinder with a six-sided polygon and a radius (R) of 30 mm is selected as the base, resulting in a stroke length (S) of 26 mm.

The stroke length of the Kresling cylinder can be divided into three states: (1) the folded state, (2) the low-energy unfolded state and (3) the high-energy unfolded state. The Kresling cylinder dissipates minimal energy during deployment between the folded state and the low-energy unfolded state. However, a clear energy jump occurs between the low-energy unfolded state and the high-energy unfolded state, attributed to the outward bending of the valley crease lines. To develop a weight-effective electromagnetic Kresling actuator, the Kresling cylinder should be unfolded towards the stroke length corresponding to the low-energy stable state (S'). A proof-of-concept Kresling cylinder was folded using 80 g m^{-2} paper. Using this cylinder, a resistance increase was noted at ¾ of the original stroke length (S). This 'low-resisting' stroke length will be considered as the effective stroke length (S') for the remainder of this study.

To determine the contraction efficiency (η) of the electromagnetic Kresling actuator, the folding resistance of the Kresling cylinder (F_{kresling}) should be determined. This was measured by manually compressing the proof-of-concept Kresling cylinder with a load cell (Futek), while the Kresling cylinder was oriented horizontally to avoid gravitational influence. This procedure was repeated 50 times, with the peak forces recorded. The average peak resistance force (F_{kresling}) was determined as 0.33 N.

2.3. Electromagnet

Generally, an electromagnetic coil is created by winding a conducting wire around a ferromagnetic core. This enhances the magnetic flux density compared to what would be achieved without the core [15]. The ferromagnetic core channels the magnetic flux, magnetizing the core, whereafter the field of the magnetized core adds to the field produced by the coil. In the case of the electromagnetic Kresling actuator, it is crucial to add limited height to the Kresling cylinder to obtain a high folding ratio. To keep the electromagnets as flat as possible, multilayer solenoidal coils were used, in which multiple layers of wires were wound around a straight cylindrical shape. Multilayer coils generate a higher magnetic field for a given current compared to a single-layer coil [15]. Equation (4) shows how the magnetic field strength (B) of a coil depends on the number of windings (N), the current (I), the coil length (L_{coil}) and the permeability of free space (μ_0). The number of windings (N) is related to the length (L_{coil}) and width (W_{coil}) of the coil and can be determined using the packing density (φ) of the wires inside the coil, see (5). The packing density

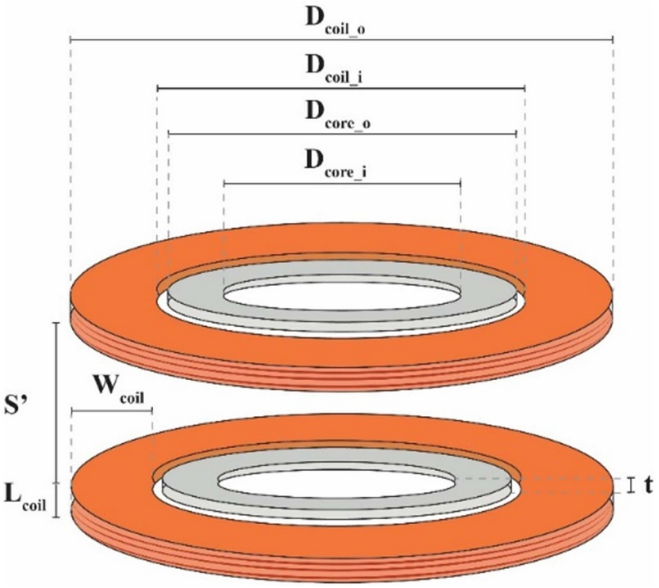

Figure 2. Geometrical setup of the electromagnets. Indicating stroke length S', coil length L_{coil}, coil width W_{coil}, core thickness t, outer coil diameter $D_{\text{coil\_o}}$, inner coil diameter $D_{\text{coil\_i}}$, outer core diameter $D_{\text{core\_o}}$ and inner core diameter $D_{\text{core\_i}}$.

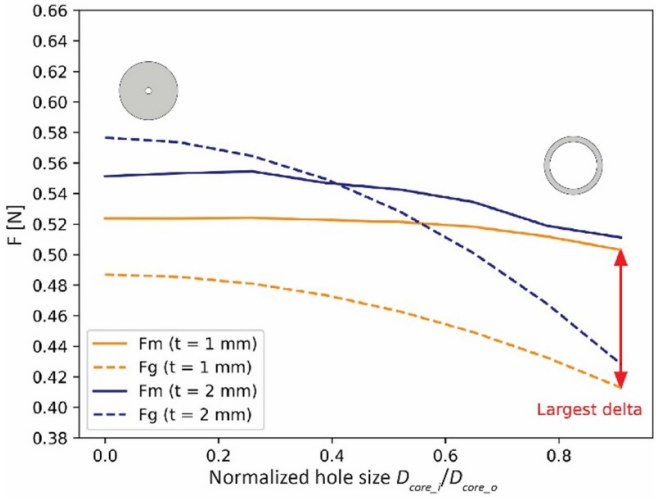

Figure 3. Effect of the inner core diameter on the electromagnetic attraction (F_{m}) and gravitational force (F_{g}) of the electromagnet. The solid lines represent the electromagnetic force, the dashed lines represent the gravitational force, the yellow lines represent a core with 1 mm thickness (t), and the blue lines represent a core with 2 mm thickness (t) .

(φ) indicates the portion of the coil's cross-section covered by the wires.

$$\boldsymbol{B} = \left(\frac{\mu_0 NI}{L_{\text{coil}}}\right)\hat{\boldsymbol{n}} \tag{4}$$

$$\varphi = \frac{A_{\text{wires}}}{A_{\text{total}}} \cdot 100\% = \frac{\pi\,(0.5D_{\text{wire}})^2 N}{L_{\text{coil}} W_{\text{coil}}} \cdot 100\%. \tag{5}$$

The challenge of designing the electromagnets to actuate the Kresling cylinder lies in bridging the relatively large gap between the two cylinder ends, since the magnetic field strength decreases rapidly with distance. This causes counteractive design choices, as larger electromagnets generate stronger electromagnetic forces, but add more weight that should be lifted during contraction. Therefore, insight into the effect of the dimensions of the separate parts of the electromagnet should be studied. The finite element analysis (FEA) was employed to simulate the electromagnetic forces between the two opposing electromagnets. In this analysis, the electromagnetic system is described by the Maxwell's equations. The material behavior is defined by the constitutive relations accounting for the macroscopic properties of the materials, considering the material permittivity ε, the material permeability μ, the material conductivity σ and the external current density $\mathbf{J_e}$. A quasi-static system was assumed. The model was used to compute the electromagnetic force generated between the electromagnets as a function of their geometric and electrical parameters. The commercial finite element software Comsol Multiphysics 6.2 was employed, combined with the AC/DC module. The model consists of 65 477 elements with mesh refinement on the cores.

Figure 2 shows the geometric setup with corresponding parameters, in which the electromagnets are represented as two identical circular, multiturn, copper coils combined with two similar iron cores. The coil is excited by a current I with a coil wire conductivity of 6×10^7 S m^{-1} and N windings. The model computes the attracting electromagnetic forces F_{m1} and F_{m2} that affect coil 1 and coil 2, respectively.

To create weight-effective electromagnets, they are designed for low mass and high magnetic attraction. The cores are modeled with varying thicknesses (t) and inner diameters ($D_{\text{core\_i}}$) to evaluate their effect on the magnetic attraction of the electromagnets, specifically the contribution of core magnetization towards the center of the core. For consistency with the proof-of-concept Kresling cylinder, the inner diameter of the coil ($D_{\text{coil\_i}}$) is set at 46 mm, while the outer diameter of the core ($D_{\text{core\_o}}$) is set at 38.5 mm to allow sufficient space for a connection mechanism between the coil and the core. The coil dimensions are standardized to isolate the effects of the core, using an 8 mm coil width (W_{coil}), a 5 mm coil length (L_{coil}), 220 windings (N) and a current (I) of 3 A. The coil weighs 36 grams. The inner diameter of the cores varies from 0 mm to 35 mm in 5 mm increments, considering cores with 1 mm and 2 mm thickness. As a result, figure 3 illustrates the relationship between the generated electromagnetic force (F_{m}) and the inner diameter of the core, and how this correlates with the gravitational force that must be overcome for full contraction. The figure shows that the electromagnetic force remains relatively stable with increasing inner diameter. This suggests that the electromagnetic force is concentrated near the coil. Conversely, an increased inner diameter significantly impacts the weight of the electromagnet. Thus, it is advantageous to employ cores with a relatively large inner diameter and low thickness, as this configuration maximizes

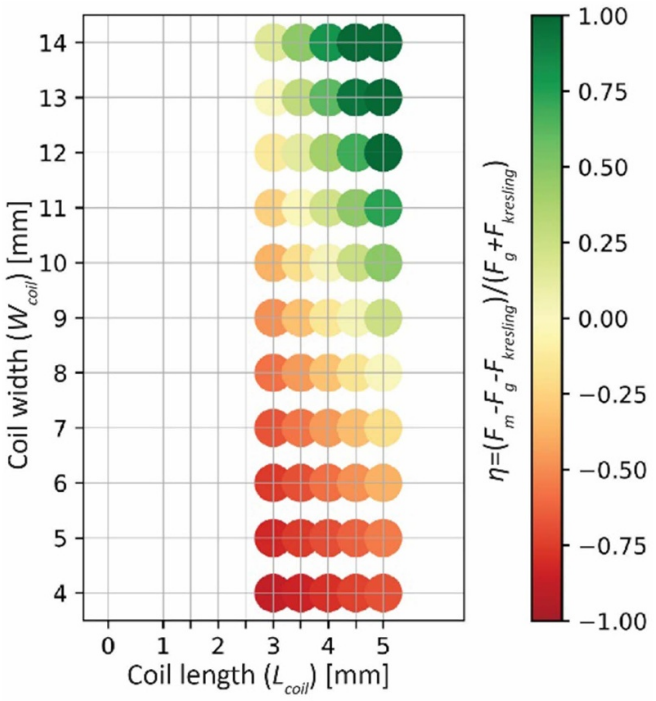

Figure 4. Effect of the coil length (L_{coil}) and coil width (W_{coil}) on the contraction efficiency (η) of the electromagnetic actuator. The color coding dictates the boundary between dimensional combinations that produce insufficient (bottom left) and sufficient (top right) contraction efficiency, the latter with a positive contraction efficiency value. F_{m} is the generated electromagnetic force, F_{g} is the associated gravitational force and F_{kresling} is the folding resistance of the Kresling cylinder.

the difference between F_{m} and F_{g}, resulting in the largest contraction efficiency (η).

To assess the impact of the coil dimensions on the contraction performance (η), different values for the coil length (L_{coil}) and coil width (W_{coil}) are considered. The influence of coil dimensions on the generated electromagnetic field requires a relationship between the number of wire windings (N), coil length (L_{coil}) and coil width (W_{coil}). To determine this, the general packing density (φ) for a coil with a 0.3 mm diameter wire is determined by counting the number of windings (N) for a manufactured coil with a 3.1 mm length (L_{coil}), 9.5 mm width (W_{coil}) and an inner radius of 23 mm. This results in 220 wire windings and a general packing density (φ) of 52.8%, following (5). It is assumed that the packing density remains constant for other coil dimensions.

The number of windings and the coil dimensions affect the total weight of the electromagnets, and consequently, the total gravitational force (F_{g}) that the electromagnets need to overcome (1). Figure 4 shows the effect of the coil length (L_{coil}) and the coil width (W_{coil}) on the contraction efficiency (η) of the electromagnetic Kresling actuator. In this model, the cores are represented as discs with a 38.5 mm outer diameter, a 35 mm inner diameter and a thickness of 1 mm. The inner diameter of the coil is set at 46 mm. The wires, with a diameter of 0.3 mm, are excited with a current of 3 A. The folding resistance of the Kresling cylinder was included to determine the contraction efficiency (η). The figure indicates that the coils must be designed with a specific combination of length (L_{coil}) and width (W_{coil}) within the green area to generate sufficient contraction efficiency (η). The FEA shows that an increased coil height and width enhances the electromagnetic force effectively offsetting the added weight during contraction.

3. Experimental validation

3.1. Model verification

The main goal of the experiments was to verify the results of the FEA model and the associated indicative design trends of the electromagnets. The performance measure was the electromagnetic force generated by sets of electromagnets with varying coil and core geometries. These measurements were compared with the expected electromagnetic force from the FEA model for those specific geometries. Six electromagnets with varying coil and core dimensions were manufactured for this purpose. The multilayer solenoidal coils were produced by winding a 0.3 mm diameter coated copper wire (Velleman) around a machined aluminium holder. The ferromagnetic cores were manufactured by laser cutting a steel plate of the desired thickness. A 3D-printed connector made from polylactic acid (PLA) was used to connect the coil and core, with the coil clamped around the cap and the core inserted into it.

The experimental setup, illustrated in figure 5, consists of two electromagnets positioned vertically with a 20 mm gap in between them. A load cell (Futek) was placed between the electromagnets to measure the generated electromagnetic force that pulls the electromagnets towards each other. The lower electromagnet was secured between two 3D-printed plates PLA, while the upper electromagnet was positioned using three guiding rails for stability and alignment. The two electromagnets were connected to two individual power supplies (VoltCraft PS-403D) with electrical clamps, using a current of 3 A. The data of the load cell was obtained using Labview. From this data, the electromagnetic force (F_{m}) was determined by subtracting the weight of the electromagnet (F_{g}) from the measured force (F_{meas}). Table 1 shows the experimental results, comparing the measured electromagnetic forces (F_{meas}) to those expected from the FEA (F_{exp}). The experimental results align with the performance trends identified using the model, even though there was a 30% error identified between the expected values from the FEA and the measured values from the experiments. This discrepancy might be caused by the imperfect packing density of the hand-wound coils, which leads to an overestimation of the electromagnetic forces. Additionally, the friction between the guiding rails and the upper electromagnet could have caused deviations. Nevertheless, the FEA still suffices for revealing general trends for electromagnet design and providing indicative estimations of how changing the core and coil dimensions affects the actuator's performance.

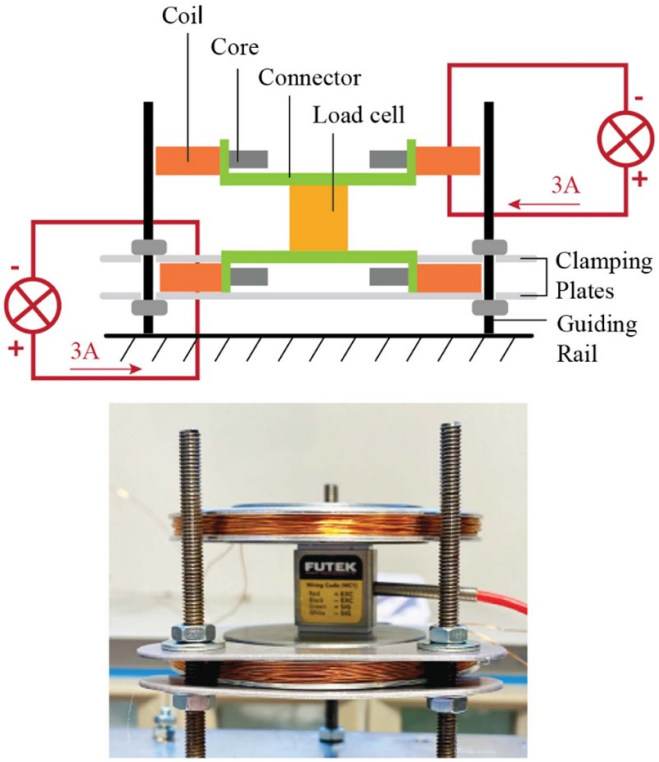

Figure 5. Experimental setup. Sets of electromagnets with varying dimensions are positioned vertically with a load cell in between to measure the generated electromagnetic force.

Table 1. The measured electromagnetic force (F_{meas}) and expected electromagnetic force (F_{exp}) for different electromagnet configurations.

N [-]	t [mm]	D_{core_i} [mm]	D_{core_o} [mm]	L_{coil} [mm]	H_{coil} [mm]	F_{meas} [N]	F_{exp} [N]
200	1	35	38.5	4.9	5.5	0.26	0.40
200	2	20	38.5	4.9	5.5	0.29	0.44
220	1	35	38.5	3.2	9.2	0.38	0.51
220	2	20	38.5	3.2	9.2	0.40	0.55
260	1	35	38.5	3.7	9.5	0.49	0.71
260	2	20	38.5	3.7	9.5	0.53	0.77

3.2. Final prototype

The FEA explored how variations on geometric parameters of the electromagnets affect the actuator performance, which resulted in trends regarding the coil and core dimensions. Following these trends from the FEA and the measured average error, a prototype of the electromagnetic Kresling actuator was manufactured within a performance-effective region to evaluate its ability to successfully contract and extend. The Kresling cylinder was constructed using 80 g m^2 paper. The coils and the cores were connected by the 3D-printed connector PLA. The Kresling cylinder was attached to the connector using glue (Pattex). The dimensions and characteristics of the final prototype are shown in table 2. The video footage in figure 6 demonstrates that the configuration of this electromagnetic Kresling actuator is able to successfully contract and extend in both horizontal orientation and vertical orientation, bearing its own weight. The prototype showcases contraction and extension within 0.2 s for both a hanging position as well as a standing position.

4. Discussion

This study presents the idea of a standalone electromagnetically-actuated Kresling actuator. The actuator consists of a Kresling cylinder positioned between two electromagnets, each composed of a copper coil and a ferromagnetic core. The embedded Kresling cylinder is of particular interest because of its bending resistance when fully unfolded, which enhances its load-bearing capacity while still allowing smooth transitions between the folded and unfolded states. An FEA was employed to analyze trends towards the dimensions of the electromagnets to effectively contract or extend the Kresling cylinder. The primary design challenge of the electromagnets lies in bridging the relatively large gap between the two ends of the Kresling cylinder, since the magnetic field strength decreases rapidly over length. Counteractive design choices need to be made, as larger electromagnets generate stronger electromagnetic forces, but add weight that should be lifted during contraction. Therefore, the main components of the electromagnets, the coil and the core,

Table 2. Details of the final prototype.

Parameter	Value	Unit	Description
L_{coil}	4.5	mm	Coil length
W_{coil}	13.5	mm	Coil width
N	450	—	Number of windings
D_{coil_i}	46	mm	Coil inner diameter
a	30	mm	Polygon side length
S'	20	mm	Effective stroke length
D_{core_o}	38.5	mm	Core outer diameter
D_{core_i}	35	mm	Core inner diameter
t	1	mm	Core thickness
m_{coil}	172.2	g	Coil weight
$m_{kresling}$	12	g	Kresling cylinder weight
$m_{connection}$	37	g	Connection weight
m_{core}	17	g	Core weight

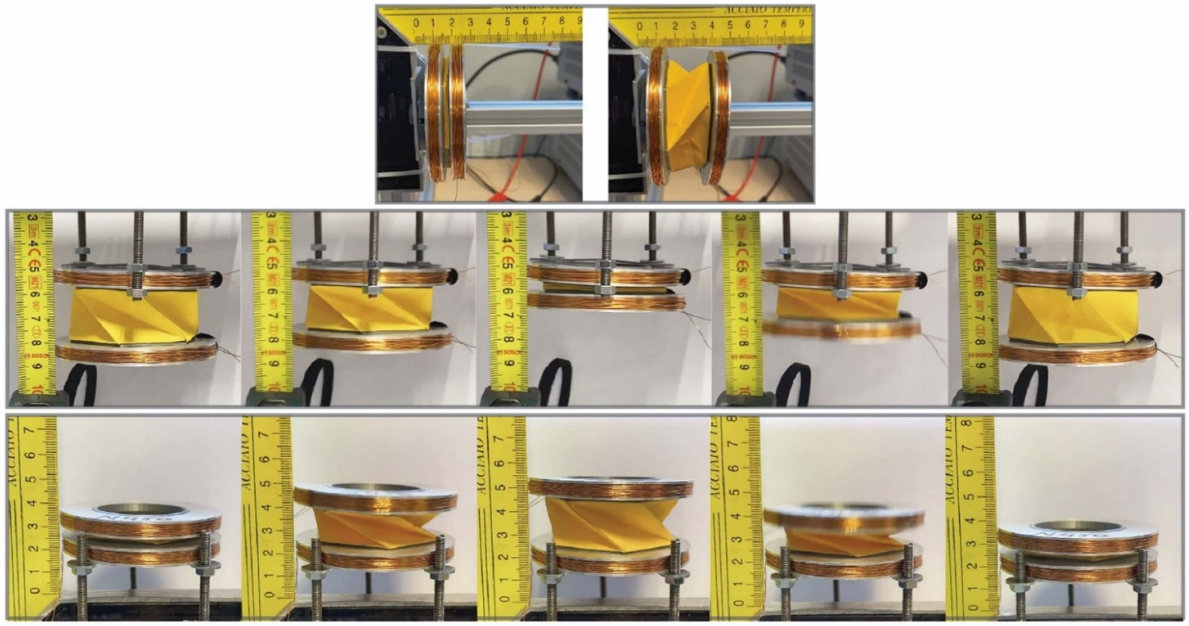

Figure 6. Contraction and extension of the prototype. Top: Linear motion in horizontal orientation. Middle: Linear motion in vertical orientation and hanging position. Bottom: Linear motion in vertical orientation and standing position.

are analyzed for low mass and high magnetic attraction to create weight-effective electromagnets. The electromagnets were designed as multilayer solenoidal coils to maintain a flat profile for easier integration into the actuator's embodiment. The observations led to a set of practical design guidelines that inform the effective design of electromagnets specifically for use in the Kresling actuator. Regarding the ferromagnetic core, the FEA indicated that increasing its inner diameter and reducing its thickness maximizes the difference between generated electromagnetic forces and the opposing weight, resulting in the largest contraction efficiency. This insight led to the design trend that reducing the core's mass, by decreasing its area and thickness, enhances contraction efficiency, with only a minimal trade-off in magnetic performance. Additionally, regarding the multilayer solenoidal coil, the FEA indicated that an increased coil height and width enhance the electromagnetic force, effectively offsetting its added weight during contraction. This insight led to the design trend that increasing the coil density enhances contraction efficiency, despite the increase in weight. Following these trends regarding the main components of the electromagnets, a prototype of the electromagnetically-actuated Kresling actuator was manufactured within a performance-effective region. The prototype successfully demonstrated contraction and extension in both horizontal and vertical directions.

Interestingly, these design guidelines for flat, weight-effective electromagnets could be employed more broadly for the implementation of embedded electromagnetic actuation into soft robots in general. Specifically, they could be valuable for incorporating embodied actuation into functional soft robotic designs.

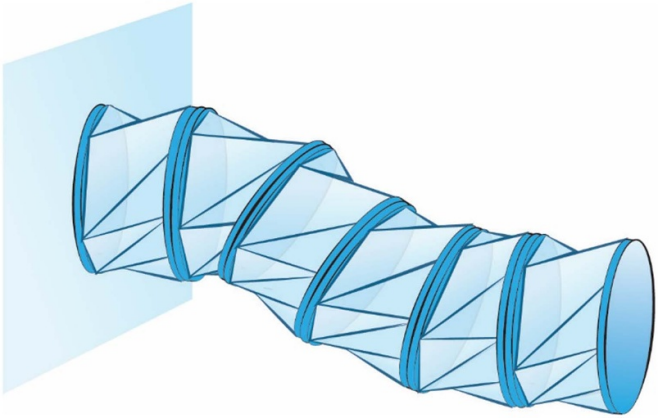

Figure 7. Impression of the electromagnetic Kresling actuator integrated into a continuum arm.

The Kresling actuator differentiates from other electromagnetic linear actuators, such as those developed by Mohamed *et al* [16] and Yin *et al* [17], by transforming its entire outer shape from a flat configuration to an extended one. This makes it specifically suitable for integration into a continuum robotic arm (figure 7). The actuator's ability to locally contract or extend based on its polarity makes it an ideal modular component, supporting a modular approach for manufacturing robotic arms. Moreover, as demonstrated by Wu *et al* [18], the Kresling cylinder has the potential to function as an omnidirectional bending actuator. Incorporating this bending capability into the electromagnetic Kresling actuator could enable the development of a modular robotic arm with precise local control over bending, contraction, and extension. It would be valuable to study the possibilities of more complex movements by simulating the actuator's full deformation, as demonstrated by Jin *et al* [19].

Additionally, the impact of scaling on the performance of the electromagnetic Kresling actuator should be examined. When the actuator is upscaled or downscaled, both the electromagnetic force and its relationship to the actuator's weight are altered. For instance, an upscaled Kresling actuator could be advantageous in logistical pick-and-place operations, where greater force and reach are needed. A downscaled version could be effective in restricted settings, such as during Minimally Invasive Surgery, where it could be attached to the tip of a catheter to enable precise needle deployment through the actuation of the electromagnets. Moreover, future research should focus on exploring the potential of the actuator's open internal lumen, which could be utilized for transporting objects or integrating tools.

5. Conclusion

In this study, we introduced a novel solution for a soft linear actuator. An electromagnetic Kresling actuator was manufactured capable of extending and contracting based on its polarity. Unlike existing solutions, the developed soft linear actuator does not suffer from bulky pneumatic components, vulnerable airtight systems or slow operational speed. Therefore, the Kresling actuator is particularly well-suited for use in dynamic, remote or restricted environments.

Future research will focus on integrating the developed actuator into a modular robotic arm and studying the effect of scaling. These additional functionalities contribute to revealing the full potential of the electromagnetic Kresling actuator, where the simple design of the manufactured prototype shows the potential for incorporating embodied actuation into functional soft robotic designs.

Data availability statement

All data that support the findings of this study are included within the article (and any supplementary files).

ORCID iDs

Vera Gesina Kortman https://orcid.org/0000-0002-2370-0013
Jouke Thomas Hompes https://orcid.org/0009-0009-3050-6532
Aimée Sakes https://orcid.org/0000-0002-4323-884X
Jovana Jovanova https://orcid.org/0000-0001-8347-6386

References

[1] Botti L, Ferrari E and Mora C 2017 Automated entry technologies for confined space work activities: a survey *J. Occup. Environ. Hyg.* **14** 271–84
[2] Hongwei L, Yan X, Zhang C and Huxiao Y 2022 Kinematic modeling and control of a novel pneumatic soft robotic arm *Chin. J. Aeronaut.* **35** 310–9
[3] Chen X, Duanmu D and Wang Z 2021 Model-based control and external load estimation of an extensible soft robotic arm *Front. Robot. AI* **7** 586490
[4] Wang W, Zhu Y, Cai S and Bao G 2023 Ultralong stretchable soft actuator (US2A): design, modeling and application *Chin. J. Mech. Eng.* **36** 13
[5] Santoso J and Onal C D 2021 An origami continuum robot capable of precise motion through torsionally stiff body and smooth inverse kinematics *Soft Robot.* **8** 371–86
[6] Novelino L S, Ze Q, Wu S, Paulino G H and Zhao R 2020 Untethered control of functional origami microrobots with distributed actuation *Proc. Natl Acad. Sci.* **117** 24096–101
[7] Li Z, Kidambi N, Wang L and Wang K-W 2020 Uncovering rotational multifunctionalities of coupled Kresling modular structures *Extreme Mech. Lett.* **39** 100795
[8] Wang X, Qu H and Guo S 2023 Tristable property and the high stiffness analysis of Kresling pattern origami *Int. J. Mech. Sci.* **256** 108515
[9] Kaufmann J, Bhovad P and Li S 2022 Harnessing the multistability of kresling origami for reconfigurable articulation in soft robotic arms *Soft Robot.* **9** 212–23
[10] Zhang C, Zhang Z, Peng Y, Zhang Y, An S, Wang Y, Zhai Z, Xu Y and Jiang H 2023 Plug & play origami modules with all-purpose deformation modes *Nat. Commun.* **14** 4329
[11] Kim J, Lee D-Y, Kim S-R and Cho K-J 2015 A self-deployable origami structure with locking mechanism induced by buckling effect *2015 IEEE Int. Conf. on Robotics and Automation (ICRA)* (IEEE) pp 3166–71
[12] Nayakanti N, Tawfick S H and Hart A J 2018 Twist-coupled kirigami cells and mechanisms *Extreme Mech. Lett.* **21** 17–24

[13] Wang X, Qu H, Li X, Kuang Y, Wang H and Guo S 2023 Multi-triangles cylindrical origami and inspired metamaterials with tunable stiffness and stretchable robotic arm *PNAS Nexus* **2** pgad098
[14] Moshtaghzadeh M, Izadpanahi E and Mardanpour P 2021 Stability analysis of an origami helical antenna using geometrically exact fully intrinsic nonlinear composite beam theory *Eng. Struct.* **234** 111894
[15] Feliziani M, Campi T, Cruciani S and Maradei F 2024 Magnetic couplers for automotive WPT systems *Wireless Power Transfer for E-Mobility: Fundamentals and Design Guidelines for Wireless Charging of Electric Vehicles* (Elsevier) pp 129–84
[16] Mohamed S, Im Y, Shin H, Kim Y and Shin B 2024 Design, modeling, and simulation of a novel electromagnetic linear actuator for linear motion *IEEE Access* **12** 38899–907
[17] Yin P, Han H, Tang L, Tan X, Guo M, Xia C and Aw K C 2024 Kresling origami-inspired electromagnetic energy harvester with reversible nonlinearity *Smart Mater. Struct.* **33** 035043
[18] Wu S, Ze Q, Dai J, Udipi N, Paulino G H and Zhao R 2021 Stretchable origami robotic arm with omnidirectional bending and twisting *Proc. Natl Acad. Sci.* **118** e2110023118
[19] Jin Y, Liu S, Li J, Cao G and Liu J 2023 Mechanical responses of soft magnetic robots with various geometric shapes: locomotion and deformation *Robotica* **41** 1203–20